Principles of a micro squeeze flow rheometer for the analysis of extremely small volumes of liquid

Journal Item

Principles of a MSFR for the analysis of extremely small volumes of liquid

D Cheneler[1], J Bowen[2], M C L Ward[1] and M J Adams[2]

[1] Department of Mechanical Engineering, University of Birmingham, Birmingham, UK
[2] Department of Chemical Engineering, University of Birmingham, Birmingham, UK

E-mail: D.Cheneler@bham.ac.uk

Abstract
In this paper, the analysis and design of a piezoelectrically actuated MSFR is presented. The fabrication of a simple prototype is described and initial experiments show the validity of the theory presented. The rheometer requires small volumes of liquid of the order of 1-10 nano-litres, and extends the frequency range an order of magnitude beyond that possible using conventional cone and plate rheometry. The electrodes of the piezoelectric disc which are used to actuate the rheometer have been patterned to allow the simultaneous measurement of the induced voltage, the phase and amplitude of which is then used to calculate the storage and loss moduli of the fluid being tested.

1. Introduction

It is well known that rheology has far reaching implications in many areas. Usually, to analyse the rheological properties of a material, conventional bulk rheometers such as cone and plate rheometers are widely used [1]. However, these rheometers due to their size, require a relatively large volume of fluid to be able to perform the analysis and so are of limited use in fields such as the analysis of biological fluids in medicine, or the prototyping of new compounds in the pharmaceutical and related industries where the amount of fluid available for analysis is small [2].

Also, the inertia of such rheometers precludes the probing of fluids at high frequencies. High frequency rheometry is useful in measuring the properties of materials at very high velocities and provides details about very short time scale relaxation processes within the molecular structure of the material. This allows for the measurement of the suspension stability in colloidal suspensions and the chain stiffness and molecular architecture in polymers etc. [3]. This information is very useful in many applications such as paint and drug synthesis and the lubrication of high speed components.

To this end there has been a concentrated effort to overcome the theoretical and technical barriers required to develop micro rheometers. A number of micro rheological techniques exist. Historically these techniques have been based around optical methods such as optical tweezers [4], single/dual particle techniques [5], dynamic light scattering [6] and the related diffusing wave spectroscopy [7].

However, while these techniques have their uses they tend to be limited to transparent and low viscosity fluids and the theoretical grounds of the techniques are still contentious [8].

Active micro rheometry also exists. Typical examples the use of include μCaBER [9] and FiSER [10] techniques for extensional rheometry and the AFM, both in force mapping mode [11] and force modulation mode [12], to measure extensional and dynamic properties of fluids. These techniques highlighted the advantages of active micro rheometry but also the need for development. It also was noticed that 'squeezing flows' frequently occur naturally in micro electromechanical systems MEMS devices [13] which led to the development of a few squeeze flow rheometers. These include the Micro Fourier Rheometer MFR [14] manufactured by GBC Scientific Melbourne, Australia, a piezoelectric axial vibrometer [15] and other more bespoke devices [16].

These devices show the potential of squeeze flow rheometry but are limited in their applicability to industrial high-throughput rheometry. However in a previous paper [17], it was shown that the storage and loss modulus of a viscoelastic liquid that can be described by the generalized Maxwell model can be calculated from the response of a MEMS device characterized in terms of its mass and stiffness. In that paper, a generic compliant oscillating squeeze flow rheometer was considered. This allowed the governing equations of motion to be derived and to be solved under the condition that the amplitude of the oscillations is kept small and that the frequency less than the resonant frequency of the device. In this paper a piezoelectrically actuated micro squeeze flow rheometer (MSFR) will be described. This rheometer has the advantage in being very small in size making it sensitive to very small volumes of liquid and light enough to operate at frequencies an order of magnitude higher than normally attainable with conventional cone and plate rheometry. Its size and the method of fabrication used also makes it very cheap to produce allowing it to be operated in parallel with a large number of similar devices. This will greatly facilitate high through-put screening of large numbers of small volumes of fluid which is necessary in the chemical and pharmaceutical industries.

The device has been analysed in terms of its electro-mechanical behaviour and it will be shown how the electrical response of the device can be used to determine the mechanical response and hence the storage and loss modulus of the liquid. The fabrication of the device will be discussed, and experimental results will be used to validate the theory.

2. The MSFR design

The rheometer consists of a partially laminated plate whereby a piezoelectric disc is bonded onto a thin silicon diaphragm (see figure 1). At the centre of the diaphragm is a small cylindrical platen directly above a similar platen which is fixed to the lower substrate (see figure 2). If a fluid is being tested, a sample consisting of a pendular bridge comprised of a viscoelastic fluid is placed between these two platens (see figure 3).

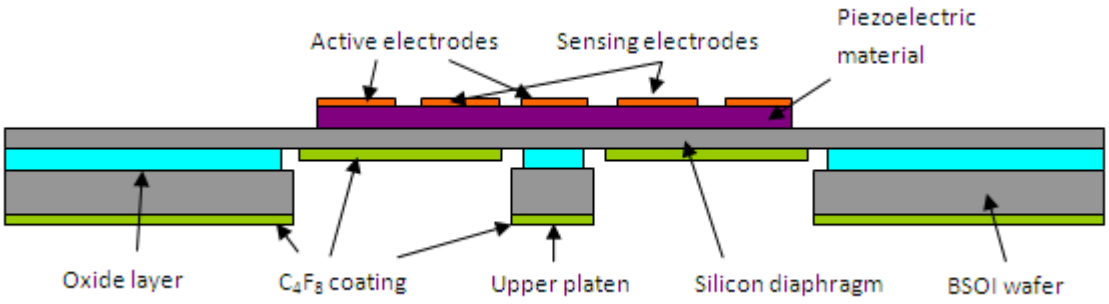

Figure 1: Schematic of the active layer of the MSFR.

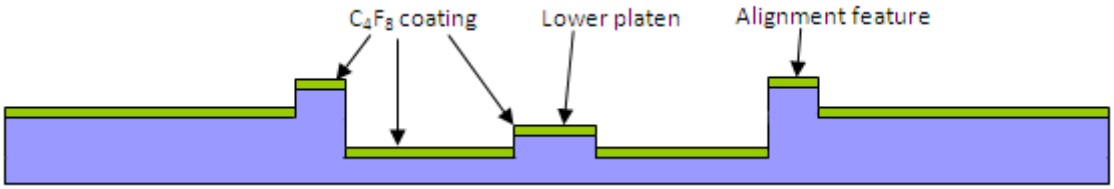

Figure 2: Schematic of the passive layer of the MSFR.

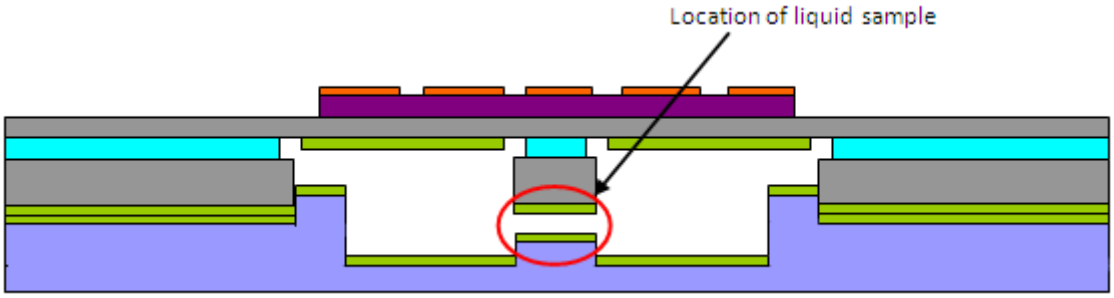

Figure 3: Schematic of the assembled MSFR.

The piezoelectric disc is partially coated with concentric electrodes which allow a potential to be applied across part of the disc, but also allows the induced voltage due to the strain in the piezoelectric material to be measured (see figure 4). The piezoelectric material is orientated in such a way as to cause it to expand radially when the potential is applied across it. This causes the silicon diaphragm to deflect, thus moving the upper platen up and down. This movement imposes a force onto the fluid thus squeezing it. The deflection of the silicon diaphragm and the piezoelectric disc due to the applied potential and the resisting force of the fluid cause a particular strain field within the piezoelectric material. This results in an induced voltage that can be measured. Given the phase and amplitude of this induced voltage, the storage and loss moduli for the viscoelastic fluid can be calculated at a range of frequencies.

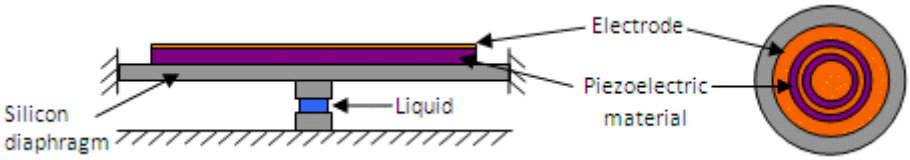

Figure 4: Schematic of the MSFR showing both profile and bird eye views.

The details for each layer in the rheometer are given below:

- The silicon diaphragm
    - The diaphragm is made out of single crystal silicon and has a low resistivity *c.a.* 0.001 Ω cm and also acts as the ground electrode for the piezoelectric material. The diaphragm has a radius of 11.5 mm and is 50 μm thick. It is assumed that it has a

Young's modulus of 170 GPa, Poisson's ratio of 0.28 and a density of 2330 kg m^{-3} [18].

- The piezoelectric material
  - This is made out of lead zirconate titanate PZT-5H. It is a disc with a 20 mm diameter and 250 μm thickness which is a commercially available size.
  - It is assumed that it has a Young's modulus of 63 GPa, Poisson's ratio of 0.3, a density of 7500 kg m^{-3} and a piezoelectric coupling coefficient d_{31} of -175x10^{-12} C/N [19].
- The electrodes
  - The PZT electrodes comprise of a 200 nm layer of silver, which has a density of 10500 kg m^{-3}, a Young's modulus of 40 GPa and a Poisson's ratio of 0.35 [19]. The electrodes were patterned to leave three concentric circles:
    - The inner electrode is an active electrode in that the input voltage will be directly applied to it. It is a circle of radius 3mm.
    - The second electrode is the sensing electrode in that the induced voltage will be measured from it. It is an annulus of inner radius 4mm and outer radius 6mm.
    - The last electrode is another active electrode. It is an annulus of inner radius 7mm and outer radius 10mm.
- The platens have a radius of 250 μm and have been coated with a fluorinated polymer film C_4F_8 so that the fluid will form a sessile drop upon depositing and not flow off the platen. The initial gap between the platens is 20 μm. These dimensions are fixed during fabrication. This sets the volume of the liquid bridge to be *c.a.* 3.9 nL. The upper platen is formed through deep reactive ion etching (DRIE) of the substrate layer of a bonded silicon on insulator (BSOI) wafer (see the Fabrication section) and so the length is fixed at 500 μm. The lower platen is formed by DRIE of a single crystal silicon wafer and so the height can be varied during fabrication. In order to give enough space for excess liquid to flow away from the platen, this height was set at 250 μm.

3. Theory

Previously it was shown that the storage G' and loss G'' modulus of a viscoelastic fluid can be calculated by considering the mechanical response of a generic MEMS device [17]. It was seen that these moduli can be determined in terms of the phase, φ, and amplitude, ε, of the oscillations of the upper platen and are functions of the mass of the active membrane of the rheometer, M, and stiffness, K_d:

$$G' = \frac{2\bar{h}^3\left[\left(F_0/\varepsilon\right)\cos\varphi + \omega^2 M - K_d + K_{cap}\right]}{3\pi\bar{R}^4} \tag{1}$$

$$G'' = \frac{2\bar{h}^3 F_0 \sin\varphi}{3\pi\varepsilon\bar{R}^4} \tag{2}$$

where $\bar{h}$ and $\bar{R}$ are the mean height and radius of the liquid bridge respectively and ω is the frequency of the oscillations in rad/s. In this case the amplitude of the applied force, F_0, is a function of the applied voltage, V_{app}, and will be discussed later. K_{cap} is the effective spring coefficient due to

the capillary force which, when the amplitude of oscillations is small, is of the form $F_{cap} = K_{cap}x(t) + c_{cap}$ and always acts to pull the upper platen downwards [17].

This shows the rheometer needs to be analysed for two purposes. The first is to ascertain the stiffness and effective mass of the moving parts of the rheometer, i.e. the silicon diaphragm, the piezoelectric disc and upper platen. The second is to find the relationship between the induced voltage and the mechanical response of the rheometer which is needed to calculate the storage and loss modulus of the liquid. Both these objectives can be achieved by calculating the shape and deflection of the silicon diaphragm when a voltage is applied across the piezoelectric layer and a point load is applied to the upper platen.

The assumptions and derivation of the deflection of the silicon diaphragm, which is based on classical laminated plate theory, closely follow the work published by Deshpande and Saggere [19]. Therefore, the reader is referred to that text rather than repeating the background theory again here. However in this case, it is assumed that the central upper platen is rigid and much smaller than the diameter of the silicon diaphragm, therefore the force exerted by the fluid manifests itself as a point load in the centre of the diaphragm. Also the potential is not applied over the entire surface of the piezoelectric disc but only across the active electrodes. Therefore the differential equations for the transverse, $w(r)$, and lateral, $u(r)$, deflection can be given instead as:

$$\left[\frac{\partial^3 w(r)}{\partial r^3} + \frac{1}{r}\frac{\partial^2 w(r)}{\partial r^2} - \frac{1}{r^2}\frac{\partial w(r)}{\partial r}\right]\left(\frac{A_{11}D_{11} - B_{11}^2}{A_{11}}\right) = \frac{P_0}{2\pi r} \tag{3}$$

$$\left[\frac{\partial^2 u(r)}{\partial r^2} + \frac{1}{r}\frac{\partial u(r)}{\partial r} - \frac{u(r)}{r^2}\right]\left(\frac{A_{11}D_{11} - B_{11}^2}{B_{11}}\right) = \frac{P_0}{2\pi r} \tag{4}$$

where $P_0/2\pi r$ is the shear force due to a point load P_0 as a function of radial distance r. A, B and D are the extensional stiffness matrix, extensional-bending coupling stiffness matrix and bending stiffness matrix as defined in [19]. The subscripts denote that it is the first element in the aforementioned matrices that are required. The solution of eqs. 3 and 4 are given as:

$$w(r) = \left(\frac{A_{11}}{A_{11}D_{11} - B_{11}^2}\right)\frac{P_0}{8\pi} r^2\left(\ln(r) - 1\right) + c_1\frac{r^2}{4} + c_2\ln(r) + c_3 \tag{5}$$

$$u(r) = \left(\frac{B_{11}}{A_{11}D_{11} - B_{11}^2}\right)\frac{P_0}{8\pi} r\left(2\ln(r) - 1\right) + c_4\frac{r}{2} + c_5\frac{1}{r} \tag{6}$$

However the rheometer is divided into four concentric areas see figure 5. The first section, denoted by α, is the inner circle as defined by the central active electrode. The next section, β, has the same material properties and layer thicknesses but the electrode is passive. The next section, γ, is another active area and δ is the bare silicon.

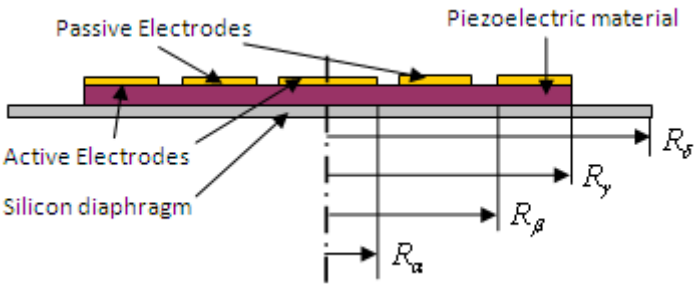

Figure 5: The concentric sections of the MSFR as denoted by their radii, R_α etc.

As there are now eight expressions describing the deflection of the diaphragm one expression for lateral and one for transverse deflection for each section, there are twenty constants of integration to solve for. Therefore the reader is referred to the Appendix for the equations for the pertinent continuity and boundary conditions. The conditions that need to be satisfied are:

1. The transverse deflection in the centre of the plate must be finite.
2. The lateral deflection in the centre of the plate must be zero.
3. The edges of the plate are fixed so the transverse and lateral deflections at the edge must be zero.
4. Similarly, the gradient of the transverse deflection must be zero at the edge.
5. At the interfaces between the sections, the deflections and gradients must be consistent.
6. Also the normal forces and bending moments acting on the interfaces must be consistent for each section.

These conditions result in the twenty expressions given in the Appendix. These equations are too lengthy and numerous to be solved algebraically but can be solved very quickly on a computer in matrix form to give the constants of integration. Given these constants, the deflection of the diaphragm due to a point load is given by c_{18}, one of the constants of integration associated with area denoted by R_α, and hence the stiffness, K_d, is easy to calculate and can be given as 48177 N/m. This would give a static deflection due to the application of 1 V as 168 nm. The shape of the silicon diaphragm is given by eq. 5. The results were compared to a finite element analysis (FEA) simulation of the rheometer as calculated using the piezoelectric sub-module in the MEMS module in Comsol Multiphysics version 3.5 (Comsol Inc. USA). In figure 6 it can be seen that this model gives very good agreement between analytical and numerical results. The slight variation between the analytical and numerical results in figure 6 is most likely due to the piecewise nature of the cross-sectional properties and hence the rigidity of the active layer. This would cause the gradients around the changes in section to have some discontinuity resulting in the discrepancy between the analytical and numerical solution.

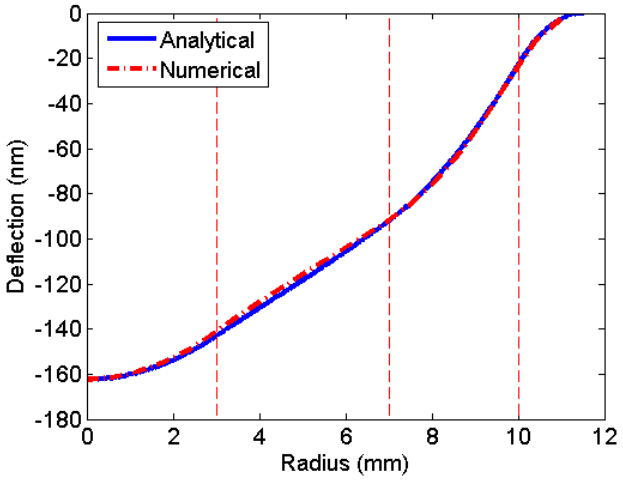

Figure 6: The shape of the silicon diaphragm when 1 V is applied to the active electrodes. The result is compared to that obtained using FEA. The vertical dashed lines correspond to the boundaries of the sections α to δ.

While these equations give the static equations of the rheometer, it is intended that the rheometer will oscillate. The dynamic equations of the diaphragm are given as [20]:

$$D_{eff}\Delta^2\Delta^2 w(r,t) = P(t) - \rho h_p \frac{\partial^2 w(r,t)}{\partial t^2} \tag{7}$$

Where D_{eff} is the effective flexural rigidity of the rheometer, $P(t)$ is the time dependent force acting on the upper platen and ρ and h_p are the effective density and thickness of the rheometer. Due to the complicated nature of the boundary and continuity conditions given in the Appendix, an analytical solution of eq. 7 is unlikely to exist. However as the amplitude of oscillations are small and the frequency is below the resonant frequency, the rheometer can be modelled as a sinusoidally oscillating mass on a spring. Therefore the effective mass, M, can be given as a function of the resonant frequency of the device, ω_0:

$$M = \frac{K_d}{\omega_0^2} \tag{8}$$

The resonant frequency of the diaphragm again is difficult to find exactly, but the Rayleigh method can be used to a reasonable accuracy. Remembering that the integrals need be solved for each section, the resonant frequency can then be given as [20]:

$$\omega_0^2 = \frac{\iint_A D_{eff}\left[\frac{\partial^2 w(r)}{\partial r^2} + \frac{1}{r}\frac{\partial w(r)}{\partial r}\right]^2 r dr d\theta}{\iint_A \rho h_p w(r)^2 r dr d\theta} \tag{9}$$

For the rheometer described above this gives the resonant frequency as 2.75 kHz The effective mass can be shown to be $1.614\text{x}10^{-4}$ kg or 25.3% of the total mass of the moving part of the rheometer. The frequency response of the rheometer given these assumptions was compared to the FE analysis of the

full 3-D structure. FEA gave the resonant frequency to be 2.9 kHz and the frequency response as shown in figure 7. This shows the method is sufficiently accurate.

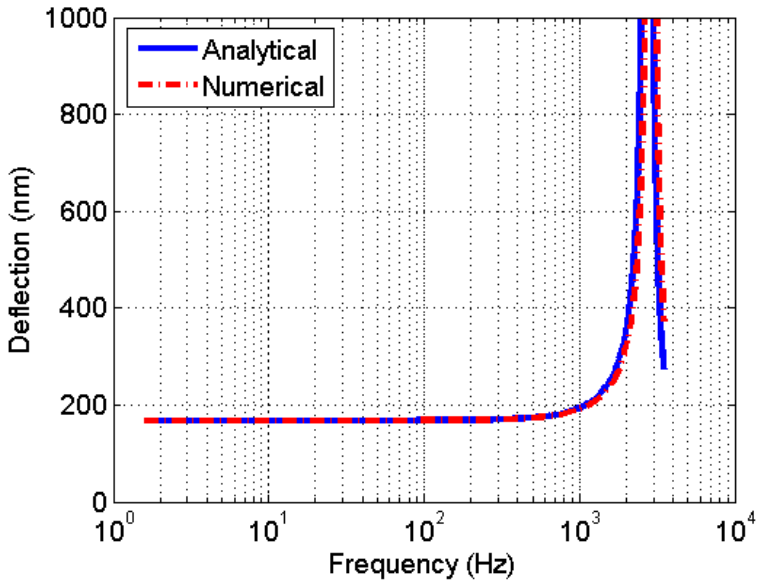

Figure 7: The frequency response of the MSFR when a voltage with amplitude of 1 V is applied to the active electrodes. The result is compared to that obtained using FEA.

The induced voltage, $v_{in}(t)$, in section β of the piezoelectric layer is due to the electric field, $E_z(z)$, induced by the strain in this region and is defined as:

$$v_{in}(t) = \int_{z_1}^{z_1+t_q} E_z(z)dz = \int_{z_1}^{z_1+t_q} q_{11}\left(\varepsilon_{rr}^k + \varepsilon_{\theta\theta}^k\right)dz \tag{10}$$

The radial, ε_{rr}^k, and tangential, $\varepsilon_{\theta\theta}^k$, strain in section β of the piezoelectric layer is defined as:

$$\begin{Bmatrix} \varepsilon_{rr}^k \\ \varepsilon_{\theta\theta}^k \end{Bmatrix} = \begin{Bmatrix} \varepsilon_{rr}^0 \\ \varepsilon_{\theta\theta}^0 \end{Bmatrix} + z_k \begin{Bmatrix} \kappa_r^0 \\ \kappa_\theta^0 \end{Bmatrix} \tag{11}$$

Where ε_{rr}^0 and $\varepsilon_{\theta\theta}^0$ are the radial and tangential strains of the reference plane, κ_r^0 and κ_θ^0 are the radial and tangential curvatures of the reference plane, respectively, as defined in [19] and z_k is the axial distance from the top of the silicon diaphragm to the top of the piezoelectric layer. The radial and tangential strain in section β of the piezoelectric layer can be shown to be:

$$\varepsilon_{rr}^k = (\Gamma - z_k\Sigma)\frac{P(t)}{8\pi}(2\ln(r)+1) + \frac{1}{2}(c_{14} - c_{11}z_k) - \frac{(c_{15} - c_{12}z_k)}{r^2} \tag{12}$$

$$\varepsilon_{\theta\theta}^k = (\Gamma - z_k\Sigma)\frac{P(t)}{8\pi}(2\ln(r)-1) + \frac{1}{2}(c_{14} - c_{11}z_k) + \frac{(c_{15} - c_{12}z_k)}{r^2} \tag{13}$$

where:

$$\Gamma = \frac{B_{\beta_{11}}}{A_{\beta_{11}} D_{\beta_{11}} - B_{\beta_{11}}^2} \quad \Sigma = \frac{A_{\beta_{11}}}{A_{\beta_{11}} D_{\beta_{11}} - B_{\beta_{11}}^2} \tag{14}$$

The subscripts denote that it is the first element in the aforementioned matrices for section β that are required. Therefore integrating eq. 10 gives the induced voltage as:

$$v_{in}(t) = q_{11} t_q \left[\left(\Gamma - \left(z_1 + \frac{t_q}{2} \right) \Sigma \right) \frac{P(t) \ln r}{2\pi} + \left(c_{14} - \left(z_1 + \frac{t_q}{2} \right) c_{11} \right) \right] \tag{15}$$

During experimentation however, what will actually be measured would be the amplitude of the induced voltage and the phase difference between the induced voltage and the applied voltage. Therefore the induced voltage would need to be separated into two parts i.e. that due to the applied voltage and that due to the resisting force of the fluid. It will be noted that in eq. 15 the applied voltage, $V(t) = V_{app} \sin \omega t$, does not appear explicitly. It does however appear in the constants of integration, which are also a function of the resisting force, $P(t) = P_0 \sin(\omega t + \alpha)$.

Remembering from eqtns. 1 and 2 that it is the amplitude and phase of the mechanical oscillations of the rheometer that is needed, eq. 15 needs to be solved in terms of the resisting force, given that the applied and induced voltages are known experimentally. This means splitting the unknown constants, c_{11} and c_{14}, into two components, one which purely a function of the applied voltage and another which is only a function of the resisting force. This would allow eq. 15 to be written in the form:

$$v_{in}(t) = V_{in} \sin(\omega t + \beta) = v_{in}^V \sin \omega t + v_{in}^P \sin(\omega t + \alpha) \tag{16}$$

where V_{in} is the amplitude and β is the phase of the induced voltage, v_{in}^V is the amplitude of the induced voltage due to the maximum applied voltage, V_{app}, and v_{in}^P is the amplitude of the induced voltage due to the maximum resisting force, P_0.

To do this, consider the boundary conditions and continuity equations given in the appendix. It is clear that they can be rearranged so that the constants of integration can be represented as:

$$[c] = [GM]^{-1} [N] \tag{17}$$

Where $[c]$ are the constants of integration, $[GM]$ is the 18 by 18 matrix made up of functions of the rheometer geometry and material properties on the LHS of the expressions in the appendix and $[N]$ is the vector made up of functions of the force and voltage on the RHS. As $[N]$ is linearly dependent on both the applied voltage and resisting force, the constants of integration can be defined in terms of other constants which are only related to either the resisting force or the applied voltage thus:

$$[c] = [GM]^{-1} \{ [F] + [Pz] \} = [GM]^{-1} \{ [F'] P(t) + [Pz'] V(t) \} \tag{18}$$

where $[F]$ and $[Pz]$ are vectors and are functions of the shear force and piezoelectric normal forces and bending moments respectively. $[F']$ and $[Pz']$ are simply $[F]$ and $[Pz]$ divided through by P_0

and V_{app} in turn. By expanding eq. 18, the constants of integration used for calculating the induced voltage can be defined in terms of resisting force and the applied voltage:

$$[c] = \left[C^1\right] P(t) + \left[C^2\right] V(t) \tag{19}$$

where $\left[C^1\right] = [GM]^{-1}[F']$ and $\left[C^2\right] = [GM]^{-1}[Pz']$.

By substituting the components of $\left[C^1\right]$ and $\left[C^1\right]$ pertaining to c_{11} and c_{14} into eq. 15 and separating into functions of $P(t)$ and $V(t)$, v_{in}^V and v_{in}^P can be defined as:

$$v_{in}^V = q_{11} t_q \left(C_{14}^2 - \left(z_1 + \frac{t_q}{2} \right) C_{11}^2 \right) V_{app} \tag{20}$$

$$v_{in}^P = q_{11} t_q \left[\left(\Gamma - \left(z_1 + \frac{t_q}{2} \right) \Sigma \right) \frac{\ln r}{2\pi} + \left(C_{14}^1 - \left(z_1 + \frac{t_q}{2} \right) C_{11}^1 \right) \right] P_0 \tag{21}$$

By rearranging eq. 16 using simple trigonometric identities and substituting in eq. 21, the amplitude, P_0, and phase, α, of the resisting force can then be shown to be:

$$P_0 = \frac{\sqrt{\left(v_{in}^V\right)^2 + \left(V_{in}\right)^2 - 2V_{in} v_{in}^V \cos\beta}}{q_{11} t_q \left[\left(\Gamma - \left(z_1 + \frac{t_q}{2} \right) \Sigma \right) \frac{\ln r}{2\pi} + \left(C_{14}^1 - \left(z_1 + \frac{t_q}{2} \right) C_{11}^1 \right) \right]} \tag{22}$$

$$\alpha = \tan^{-1} \left(\frac{-V_{in} \sin\beta}{v_{in}^V - V_{in} \cos\beta} \right) \tag{23}$$

where r is now the distance to the centre of the passive electrode i.e. 5 mm. This force now needs to be related to the amplitude of the mechanical oscillations of the platen, so that eqtns. 1 and 2 can be calculated. The derivation of eqtns. 1 and 2 were given in [17] where it was shown that the mechanics of the rheometer can be described by a force balance resulting in a second order differential equation. It was also shown that if the amplitude of the applied force, F_0, was small, the resulting motion was sinusoidal and can be expressed in the following form:

$$F_0 \sin\omega t + P_0 \sin(\omega t + \alpha) = \varepsilon \sin(\omega t + \varphi) \left(K_d - K_{cap} \right) \tag{24}$$

where ε, is the amplitude, φ, is the phase of the oscillations of the central platen respectively. The deflection of the centre of the silicon diaphragm is given by eq. 5 when the material properties pertain to section α and r = 0. It can therefore be seen that the deflection is described by the constant of integration c_{18} as calculated in eq. 17. By considering the force required to deflect the diaphragm by an amount c_{18} as given by $F = K_d c_{18}$ and the LHS of eq. 24, the amplitude can be given as:

$$\varepsilon = c_{18}\left(\frac{K_d}{K_d - K_{cap}}\right) \tag{25}$$

Similarly, by applying a simple trigonometric identity to eq. 24, the phase can be found:

$$\varphi = \tan^{-1}\left(\frac{P_0 \sin\alpha}{F_0 + P_0 \cos\alpha}\right) \tag{26}$$

Equation (25) shows how the capillary force of the liquid bridge decreases the stiffness of the rheometer. The only variable that has not yet been defined is the effective force due to the applied voltage, F_0. As stated before, the deflection of the centre of the diaphragm is given by c_{18}. It was shown in eq. 19 that these constants are independent linear functions of both the resisting force and voltage. The deflection due purely to an applied voltage is given by eq. 19 as:

$$c_{18} = C_{18}^2 V(t) \tag{27}$$

As the effect of applying a force or a voltage is the same, the applied voltage can be considered to be an effective applied force, $F_0 \sin\omega t$. Again as the force required to deflect the diaphragm by an amount c_{18} as given by $F = K_d c_{18}$, F_0 can be defined as:

$$F_0 = K_d C_{18}^2 V_{app} \tag{28}$$

With these values, the original expressions for the storage and loss moduli as given in eqs. 1 and 2 can be solved.

4. Fabrication

In order to verify the theory and the effectiveness of the proposed MSFR, prototypes of the rheometer were fabricated. Figure 8 shows the fabrication steps for the active part of the rheometer which consists of the diaphragm, piezoelectric layer and upper platen as shown in figure 1. It is based on a BSOI wafer (Si-Mat, Germany) with a 50 μm thick device layer with a resistivity of *c.a.* 0.001 Ω cm on a 500 μm handle wafer with a 2 μm oxide layer in between. First, the bottom of the handle wafer is patterned with a 9 μm layer of SPR 220-7 (Chestech, UK) to define a series of thin concentric rings between the upper platen and edge of the diaphragm. Next, the handle wafer is etched through to expose the underlying oxide using a STS Multiplex ICP DRIE etcher (STS Plc., UK). This will leave the concentric rings connected to the oxide. These are necessary to support the diaphragm during the subsequent processes but are removed later. The PZT-5H discs (Physik Instrumente GmbH & Co., Germany) were purchased already coated with silver electrodes on both sides and was 20 mm in diameter and 250 μm thick. Both sides of the discs were then coated with a 9 μm layer of SPR 220-7 and one side patterned to expose the gaps between the electrodes. The excess silver was then etched away by submerging the PZT in nitric acid. The resist was removed and the disc was glued on to the centre of the silicon diaphragm. The supporting silicon rings were then removed by removing the underlying oxide by submerging the area in HF acid. Care was taken not to undercut the upper platen too much and cause it to be released. The underside of the handle wafer and upper platen were then coated with a 250 nm thick layer of C_4F_8, for reasons discussed above, by depositing gas-polymerized C_4F_8 at a flow rate of 80 sccm for 1 minute 23 seconds in the STS Multiplex ICP DRIE etcher.

Figure 9 shows the fabrication of the passive layer which comprises of the lower platen, a sunken area to allow excess fluid to flow away and alignment features as shown in figure 2. It is made from a 525 μm thick single crystal silicon wafer (Si-Mat, Germany). As can be seen the features are defined by etching down using the STS Multiplex ICP DRIE etcher to three different heights. In each step the area was first patterned using a 9 μm layer of SPR 220-7 and standard photolithography techniques, before being etched to the required depth using the STS Multiplex ICP DRIE etcher. The first etch was to a depth of 100 μm to define the alignment marks. The second was to 120.5 μm to define the gap between the platens, the last etch was a further 250 μm which was to give enough space for excess liquid to flow away from the platen. In a manner similar to before, the whole surface was coated with a 250 nm thick layer of C_4F_8 by depositing gas-polymerized C_4F_8 at a flow rate of 80 sccm for 1 minute 23 seconds in the STS Multiplex ICP DRIE etcher. For assembly, before experimentation, a liquid drop is placed on the lower platen and the upper part of the rheometer is brought down into contact with the lower part and clamped together. The alignment feature, which is simply a raised ring which fits inside the edge of the diaphragm, ensures the platens are aligned.

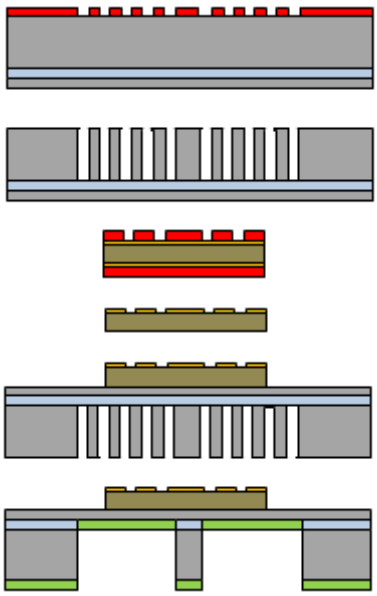

Figure 8: Fabrication steps of the upper part of the MSFR as shown in figure 1. The red denotes photoresist, the grey is silicon, the blue is the oxide layer, the brown is PZT, the gold denotes the silver electrodes and the green is the C_4F_8 layer.

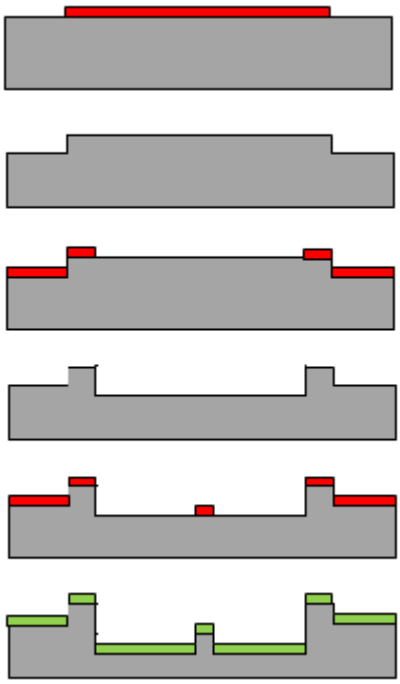

Figure 9: Fabrication steps of the lower part of the MSFR as shown in figure 2. The colours denote the same material as stated in figure 8.

5. Experiment

In order to check the accuracy of the microrheometer it was necessary to compare the results to those obtained by conventional oscillatory rheometry. Therefore, the storage and loss moduli of PDMS of viscosities 10 Pa s, 30 Pa s and 340 Pa s (Dow Corning, USA) were obtained using an AR2000 cone and plate rheometer (TA instruments, USA). PDMS was used as it is a well known polymer consisting of a linear molecule which can be accurately and repeatably synthesized to the required viscosity. PDMS also exhibits low volatility and hence is suitable for measurements where extremely small volumes of liquid are required. For the rheometry measurements a 20 mm stainless steel truncated cone with a 4° side wall angle was used to manipulate the liquid. A frequency sweep from 0.1 Hz to 100 Hz where possible was performed with logarithmic increments. The amplitude of the applied strain angle of twist multiplied by the radius of the sample divided by average height was kept constant at 1 %. The sample volume was approximately 0.15 mL and the sample temperature was set to 25 °C maintained by a Peltier plate. Assuming that the generalized Maxwell model describes these fluids sufficiently over the frequency range of interest, the measured cone and plate data were used to calculate the elastic, G, and viscous, η, coefficients used in the model using a least-square method of curve fitting. These coefficients are related to the storage and loss moduli by the relationships [21]:

$$G' = \sum_{i=0}^{n} \frac{\eta_i \lambda_i \omega^2}{1+\omega^2 \lambda_i^{\,2}} \quad \text{and} \quad G'' = \sum_{i=0}^{n} \frac{\eta_i \omega}{1+\omega^2 \lambda_i^{\,2}} \tag{29}$$

The low viscosity fluids are adequately represented by a single element, but the higher viscosity fluids exhibit more relaxation processes and require more elements. The elastic and viscous coefficients and the associated time constants, λ, for the various liquids are given in table 1:

Table 1: The Maxwell properties for a range of liquids as calculated from the cone and plate data. η is the dynamic viscosity, G is the shear modulus and λ is the relaxation time.

Fluid	Parameter	Element 1	Element 2	Element 3	Element 4
340 Pa s PDMS	η Pa.s	63.018	91.753	71.774	72.591
	G Pa	62854.046	2313.821	13743.306	4681.638
	λ s	0.00100	0.0397	0.00522	0.0155
30 Pa s PDMS	η Pa.s	26.426	-	-	-
	G Pa	10891.387	-	-	-
	λ s	0.00242	-	-	-
10 Pa s PDMS	η Pa.s	9.773	-	-	-
	G Pa	21138.806	-	-	-
	λ s	0.0004624	-	-	-

The MSFR was tested as follows: First the base plate was placed under a microscope and a drop applied to the lower platen by dipping a glass rod into the liquid and placing the liquid onto the platen. The active plate was then assembled onto the base plate and electrical probes were placed in contact with the pertinent electrodes.

The rheometer was excited by applying a sinusoidal voltage with constant amplitude of 1 V using a function generator. The frequency was varied on a logarithmic scale from 10Hz to 1000Hz. The voltage was applied directly to the rheometer by placing probes attached to coaxial cable onto the active electrodes on the piezoelectric material on the rheometer. The passive electrode was connected through a unity gain buffer amplifier, to negate impedance effects, to an ADC-212 Picoscope, a virtual oscilloscope by Pico Inc. The input voltage and induced voltage were recorded simultaneously by the Picoscope. The data was then analysed to find the amplitude of the induced voltage and phase difference between the input and induced voltage as a function of frequency. The phase and amplitude of the induced voltage for a range of liquids are shown in figures 10 and 11.

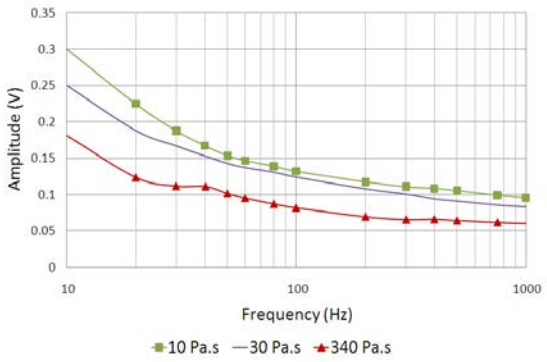

Figure 10: The frequency response of the amplitude of the induced voltage for a range of fluids.

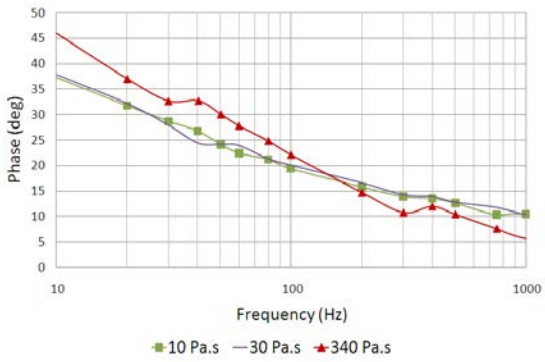

Figure 11: The frequency response of the phase difference of the induced voltage for a range of fluids.

The model described in Section 3 was applied to the data given in figures. 10 and 11 to calculate the storage and loss moduli as measured by the MSFR. The results were compared the data given by the

cone and plate rheometry. In order to predict the fluid response at higher frequencies it was assumed that the Maxwell model was applicable to a frequency of 1 kHz. Moduli were extrapolated by applying eq. 29 to the constants given in Table 1. Results are shown for PDMS with zero shear viscosities of 10 Pa s (figures 12-13), 30 Pa s (figures 13-14) and 340 Pa s (figures 15-16):

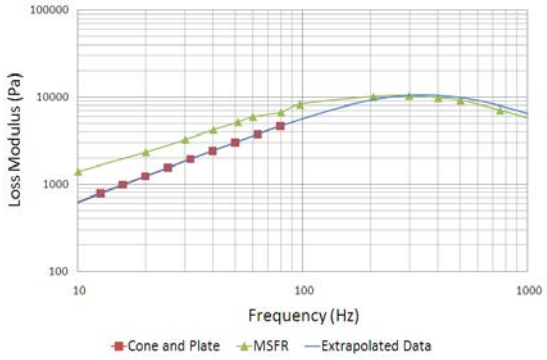

Figure 12: Loss moduli for 10 Pa s PDMS obtained from cone and plate rheometry, the MSFR and extrapolated data [22].

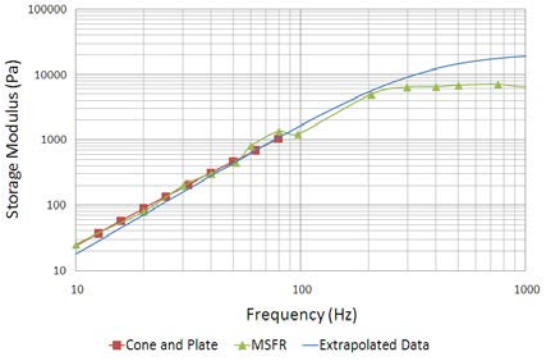

Figure 13: Storage moduli for 10 Pa s PDMS obtained from cone and plate rheometry, the MSFR and extrapolated data [22].

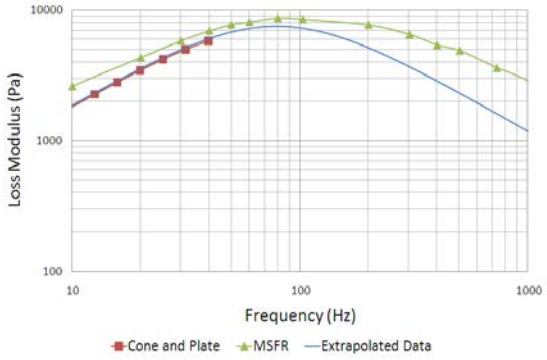

Figure 14: Loss moduli for 30 Pa s PDMS obtained from cone and plate rheometry, the MSFR and extrapolated data.

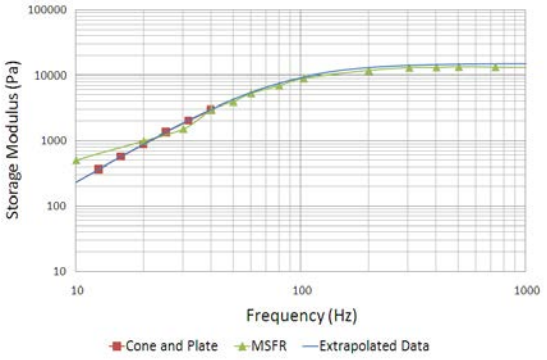

Figure 15: Storage moduli for 30 Pa s PDMS obtained from cone and plate rheometry, the MSFR and extrapolated data.

Figures 12-15 show that the data obtained from the MSFR for PDMS fluids of zero shear viscosity 10 Pa s and 30 Pa s are in close agreement with the measured cone and plate data for the low frequency regime, and in reasonable agreement with the values extrapolated from the generalized Maxwell model for the high frequency regime. This suggests the MSFR behaves as suggested in Section 3 and is therefore a potentially useful tool for measuring high frequency properties of nano-litre volumes of viscoelastic fluids. Deviations from expected results are most likely due to inaccuracies in the prototype fabrication and noise in the associated circuitry. It is expected that correlation should improve given optimisation of these factors. However at this stage, it is premature to draw any quantitative conclusions on the rheometry at high frequencies.

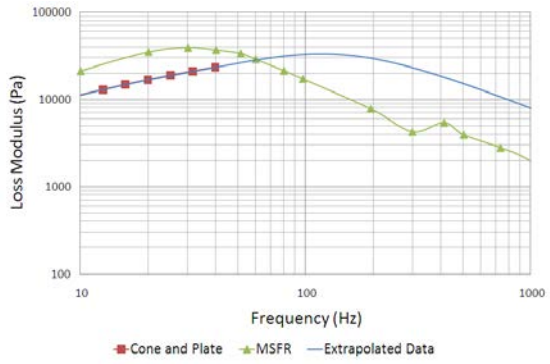

Figure 16: Loss moduli for 340 Pa s PDMS obtained from cone and plate rheometry, the MSFR and extrapolated data.

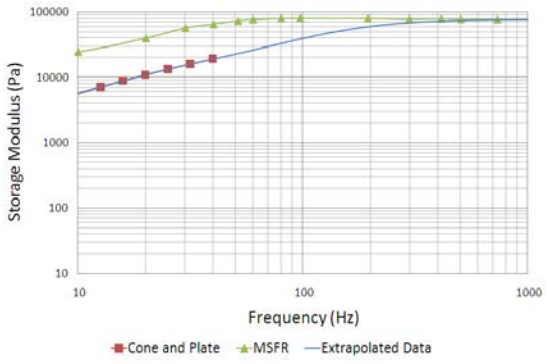

Figure 17: Storage moduli for 340 Pa s PDMS obtained from cone and plate rheometry, the MSFR and extrapolated data.

Figures 16-17 reveal that the magnitude of the moduli measured for PDMS with zero shear viscosity 340 Pa s is in good qualitative agreement with the values extrapolated from the generalized Maxwell model, but the frequency scale appears to have shifted. The most likely cause for this discrepancy, given the agreement shown in figures 12 to 15, is excess liquid surrounding the platens. It was stated above that the liquid was applied to the MSFR using a glass rod to place a sessile drop on the lower platen. If the platen is filled, this drop will have a larger volume than the liquid bridge formed between the platens when the MSFR is assembled, assuming the excess liquid has drained away off the platen due to gravity. Given the viscosity of this liquid it is possible that it did not completely drain away from the platens, and hence excess liquid remained in contact with the measurement region. This would cause the geometry of the sample to differ from that assumed in the theory resulting in erroneous moduli to be calculated. This is consistent with the data shown in figures 16 and 17 in that the fluid properties measured appear to be in agreement with the cone and plate data and the extrapolated values, but shifted along the frequency axis somewhat. This effect is speculative however, and the effect is not completely understood at this point.

Figs. 12-17 show that the MSFR can be used to measure the storage and loss moduli of very small volumes of viscoelastic liquids to frequencies an order of magnitude larger than conventional cone and plate rheometry. The figures also suggest that the model outlined in this work is valid and reasonably accurate. The generalized Maxwell model was chosen in preference to the Rouse model for describing the behaviour of the high molecular weight fluids which the MSFR would be used to measure. The Rouse model is suited to dilute polymer solutions and low molecular weight polymer melts [23]. The PDMS fluids employed in this work have molecular weights above the PDMS critical entanglement molecular weight of 34 kg/mol [24], which is why they exhibit viscoelastic behaviour, and therefore the Rouse model is an inappropriate choice for describing its rheological behaviour.

6. Conclusion

In this paper a design for a MSFR has been presented. The design incorporates a piezoelectric disc for both sensing and actuation. The mechanics and operation of the rheometer has been analysed in detail and incorporated with previous work detailing the use of MEMS for conducting squeeze flow

rheometry. It has been shown that the theory agrees very well with numerical simulations. It has also been shown that it allows experiments which produce data which is comparable with conventional cone and plate rheological data at lower viscosities although there discrepancies for the case of 340 Pa.s PDMS, although this is most likely due to the quality of the prototype. It has also been shown that the MSFR requires a sample size of the order of nanolitres which is a much smaller volume of fluid than cone and plate rheometry requires. It also extends the frequency range at which fluids can be tested an order of magnitude beyond the capabilities of cone and plate rheometry.

Acknowledgments
The University of Birmingham and Unilever Research & Development are acknowledged for financial support for JB and DC. The authors are grateful to Geraint Roberts at Unilever Port Sunlight for his assistance with performing and interpreting rheometry measurements.

Appendix: The Boundary Conditions and Continuity Equations for the Rheometer

Here the equations representing the boundary conditions and the continuity equations ensuring consistency in the deflections, gradients, normal forces and bending moments between the sections of the rheometer as defined in the theory section above are given. It is intended that these simultaneous linear equations are solved in matrix form in order to give the constants required to solve eq. 5 and 6 for the deflection of the rheometer.

- At $r = 0,\ w$ and u must be finite:
  Therefore c_{17} and c_{20} must equal zero
- At $r = R_\delta, w_\delta = 0$ therefore:

$$c_1 \frac{R_\delta^2}{4} + c_2 \ln\left(R_\delta\right) + c_3 = \frac{A_{\delta_{11}}}{A_{\delta_{11}} D_{\delta_{11}} - B_{\delta_{11}}^2} \frac{P}{8\pi} R_\delta^2 \left(\ln\left(R_\delta\right) - 1\right) \tag{A.1}$$

- At $r = R_\delta, \dfrac{dw_\delta}{dr} = 0$ therefore:

$$c_1 \frac{R_\delta}{2} + c_2 \frac{1}{R_\delta} = \frac{A_{\delta_{11}}}{A_{\delta_{11}} D_{\delta_{11}} - B_{\delta_{11}}^2} \frac{P}{8\pi} R_\delta \left(2\ln\left(R_\delta\right) - 1\right) \tag{A.2}$$

- At $r = R_\delta, u_\delta = 0$ therefore:

$$c_4 \frac{R_\delta}{2} + c_5 \frac{1}{R_\delta} = \frac{B_{\delta_{11}}}{A_{\delta_{11}} D_{\delta_{11}} - B_{\delta_{11}}^2} \frac{P}{8\pi} R_\delta \left(2\ln\left(R_\delta\right) - 1\right) \tag{A.3}$$

- At $r = R_\gamma, w_\delta = w_\gamma$ therefore:

$$\begin{aligned} &c_1 \frac{R_\gamma^2}{4} + c_2 \ln\left(R_\gamma\right) + c_3 - c_6 \frac{R_\gamma^2}{4} - c_7 \ln\left(R_\gamma\right) - c_8 = \\ &\left[\left(\frac{A_{\gamma_{11}}}{A_{\gamma_{11}} D_{\gamma_{11}} - B_{\gamma_{11}}^2}\right) - \left(\frac{A_{\delta_{11}}}{A_{\delta_{11}} D_{\delta_{11}} - B_{\delta_{11}}^2}\right)\right] \frac{P}{8\pi} R_\gamma^2 \left(\ln\left(R_\gamma\right) - 1\right) \end{aligned} \tag{A.4}$$

- At $r = R_\gamma, \frac{dw_\delta}{dr} = \frac{dw_\lambda}{dr}$ therefore:

$$c_1 \frac{R_\gamma}{2} + c_2 \frac{1}{R_\gamma} - c_6 \frac{R_\gamma}{2} - c_7 \frac{1}{R_\gamma} = \left[\left(\frac{A_{\lambda_{11}}}{A_{\lambda_{11}} D_{\lambda_{11}} - B_{\lambda_{11}}^2} \right) - \left(\frac{A_{\delta_{11}}}{A_{\delta_{11}} D_{\delta_{11}} - B_{\delta_{11}}^2} \right) \right] \frac{P}{8\pi} R_\gamma \left(2\ln\left(R_\gamma\right) - 1 \right) \tag{A.5}$$

- At $r = R_\lambda, u_\delta = u_\gamma$ therefore:

$$c_4 \frac{R_\gamma}{2} + c_5 \frac{1}{R_\gamma} - c_9 \frac{R_\gamma}{2} - c_{10} \frac{1}{R_\gamma} = \left[\left(\frac{B_{\gamma_{11}}}{A_{\gamma_{11}} D_{\gamma_{11}} - B_{\gamma_{11}}^2} \right) - \left(\frac{B_{\delta_{11}}}{A_{\delta_{11}} D_{\delta_{11}} - B_{\delta_{11}}^2} \right) \right] \frac{P}{8\pi} R_\gamma \left(2\ln\left(R_\gamma\right) - 1 \right) \tag{A.6}$$

- At $r = R_\lambda, N_{r_\delta} = N_{r_\gamma}$, where N_r denotes the radial normal force, therefore:

$$\begin{aligned} &\left(\frac{B_{\delta_{11}} + B_{\delta_{12}}}{-2} \right) c_1 + \left(\frac{B_{\delta_{11}} - B_{\delta_{12}}}{R_\gamma^2} \right) c_2 + \left(\frac{A_{\delta_{11}} + A_{\delta_{12}}}{2} \right) c_4 + \left(\frac{A_{\delta_{12}} - A_{\delta_{11}}}{R_\gamma^2} \right) c_5 + \\ &\left(\frac{B_{\gamma_{11}} + B_{\gamma_{12}}}{2} \right) c_6 - \left(\frac{B_{\gamma_{11}} - B_{\gamma_{12}}}{R_\gamma^2} \right) c_7 - \left(\frac{A_{\gamma_{11}} + A_{\gamma_{12}}}{2} \right) c_9 - \left(\frac{A_{\gamma_{12}} - A_{\gamma_{11}}}{R_\gamma^2} \right) c_{10} = \\ &\left[\left(\frac{A_{\gamma_{12}} B_{\gamma_{11}} - A_{\gamma_{11}} B_{\gamma_{12}}}{A_{\gamma_{11}} D_{\gamma_{11}} - B_{\gamma_{11}}^2} \right) - \left(\frac{A_{\delta_{12}} B_{\delta_{11}} - A_{\delta_{11}} B_{\delta_{12}}}{A_{\delta_{11}} D_{\delta_{11}} - B_{\delta_{11}}^2} \right) \right] \frac{P}{8\pi} \left(2\ln\left(R_\gamma\right) - 1 \right) - N_r^P \end{aligned} \tag{A.7}$$

N_r^P denotes the radial normal force in the piezoelectric layer due to the applied voltage. It is given in [19] as: $N_r^P = \frac{(1+\nu_p)E_p}{(1-\nu_p)^2} d_{31} V(t)$, where ν_p, E_p and d_{31} are the Poisson's ratio, Young's modulus and piezoelectric coupling coefficient of the piezoelectric material as defined in section 2.

- At $r = R_\gamma, M_{r_\delta} = M_{r_\gamma}$, where M_r denotes the radial bending moment, therefore:

$$\begin{aligned} &\left(\frac{D_{\delta_{11}} + D_{\delta_{12}}}{-2} \right) c_1 + \left(\frac{D_{\delta_{11}} - D_{\delta_{12}}}{R_\gamma^2} \right) c_2 + \left(\frac{B_{\delta_{11}} + B_{\delta_{12}}}{2} \right) c_4 + \left(\frac{B_{\delta_{12}} - B_{\delta_{11}}}{R_\gamma^2} \right) c_5 + \\ &\left(\frac{D_{\gamma_{11}} + D_{\gamma_{12}}}{2} \right) c_6 - \left(\frac{D_{\gamma_{11}} - D_{\gamma_{12}}}{R_\gamma^2} \right) c_7 - \left(\frac{B_{\gamma_{11}} + B_{\gamma_{12}}}{2} \right) c_9 - \left(\frac{B_{\gamma_{12}} - B_{\gamma_{11}}}{R_\gamma^2} \right) c_{10} = \\ &\left[\left(\frac{B_{\gamma_{11}} B_{\gamma_{11}} - A_{\gamma_{11}} D_{\gamma_{11}}}{A_{\gamma_{11}} D_{\gamma_{11}} - B_{\gamma_{11}}^2} \right) - \left(\frac{B_{\delta_{11}} B_{\delta_{11}} - A_{\delta_{11}} D_{\delta_{11}}}{A_{\delta_{11}} D_{\delta_{11}} - B_{\delta_{11}}^2} \right) \right] \frac{P}{8\pi} \left(2\ln\left(R_\gamma\right) + 1 \right) + \\ &\left[\left(\frac{B_{\gamma_{11}} B_{\gamma_{12}} - A_{\gamma_{11}} D_{\gamma_{12}}}{A_{\gamma_{11}} D_{\gamma_{11}} - B_{\gamma_{11}}^2} \right) - \left(\frac{B_{\delta_{11}} B_{\delta_{12}} - A_{\delta_{11}} D_{\delta_{12}}}{A_{\delta_{11}} D_{\delta_{11}} - B_{\delta_{11}}^2} \right) \right] \frac{P}{8\pi} \left(2\ln\left(R_\gamma\right) - 1 \right) - M_r^P \end{aligned} \tag{A.8}$$

M_r^P denotes the radial bending moment in the piezoelectric layer due to the applied voltage. It is given in [19] as: $M_r^P = \frac{1}{2}\frac{(1+\nu_p)E_p}{(1-\nu_p)^2}\frac{V(t)}{t_p}d_{31}\left(z_1^2 - z_2^2\right)$, where t_p is the thickness of the of the piezoelectric material as defined in section 2 and z_1 is the distance from the neutral axis of the silicon diaphragm to bottom of the piezoelectric layer and $z_2 = z_1 + t_p$.

- At $r = R_\beta, w_\gamma = w_\beta$ therefore:

$$c_6\frac{R_\beta^2}{4} + c_7\ln\left(R_\beta\right) + c_8 - c_{11}\frac{R_\beta^2}{4} - c_{12}\ln\left(R_\beta\right) - c_{13} = \left[\left(\frac{A_{\beta_{11}}}{A_{\beta_{11}}D_{\beta_{11}} - B_{\beta_{11}}^2}\right) - \left(\frac{A_{\gamma_{11}}}{A_{\gamma_{11}}D_{\gamma_{11}} - B_{\gamma_{11}}^2}\right)\right]\frac{P}{8\pi}R_\beta^2\left(\ln\left(R_\beta\right) - 1\right) \tag{A.9}$$

- At $r = R_\beta, \frac{dw_\gamma}{dr} = \frac{dw_\beta}{dr}$ therefore:

$$c_6\frac{R_\beta}{2} + c_7\frac{1}{R_\beta} - c_{11}\frac{R_\beta}{2} - c_{12}\frac{1}{R_\beta} = \left[\left(\frac{A_{\beta_{11}}}{A_{\beta_{11}}D_{\beta_{11}} - B_{\beta_{11}}^2}\right) - \left(\frac{A_{\lambda_{11}}}{A_{\lambda_{11}}D_{\lambda_{11}} - B_{\lambda_{11}}^2}\right)\right]\frac{P}{8\pi}R_\beta\left(2\ln\left(R_\beta\right) - 1\right) \tag{A.10}$$

- At $r = R_\beta, u_\gamma = u_\beta$ therefore:

$$c_9\frac{R_\beta}{2} + c_{10}\frac{1}{R_\beta} - c_{14}\frac{R_\beta}{2} - c_{15}\frac{1}{R_\beta} = \left[\left(\frac{B_{\beta_{11}}}{A_{\beta_{11}}D_{\beta_{11}} - B_{\beta_{11}}^2}\right) - \left(\frac{B_{\gamma_{11}}}{A_{\gamma_{11}}D_{\gamma_{11}} - B_{\gamma_{11}}^2}\right)\right]\frac{P}{8\pi}R_\beta\left(2\ln\left(R_\beta\right) - 1\right) \tag{A.11}$$

- At $r = R_\beta, N_{r_\gamma} = N_{r_\delta}$ therefore:

$$\left(\frac{B_{\gamma_{11}} + B_{\gamma_{12}}}{-2}\right)c_6 + \left(\frac{B_{\gamma_{11}} - B_{\gamma_{12}}}{R_\beta^2}\right)c_7 + \left(\frac{A_{\gamma_{11}} + A_{\gamma_{12}}}{2}\right)c_9 + \left(\frac{A_{\gamma_{12}} - A_{\gamma_{11}}}{R_\beta^2}\right)c_{10} + \left(\frac{B_{\beta_{11}} + B_{\beta_{12}}}{2}\right)c_{11} - \left(\frac{B_{\beta_{11}} - B_{\beta_{12}}}{R_\beta^2}\right)c_{12} - \left(\frac{A_{\beta_{11}} + A_{\beta_{12}}}{2}\right)c_{14} - \left(\frac{A_{\beta_{12}} - A_{\beta_{11}}}{R_\beta^2}\right)c_{15} = \left[\left(\frac{A_{\beta_{12}}B_{\beta_{11}} - A_{\beta_{11}}B_{\beta_{12}}}{A_{\beta_{11}}D_{\beta_{11}} - B_{\beta_{11}}^2}\right) - \left(\frac{A_{\gamma_{12}}B_{\gamma_{11}} - A_{\gamma_{11}}B_{\gamma_{12}}}{A_{\gamma_{11}}D_{\gamma_{11}} - B_{\gamma_{11}}^2}\right)\right]\frac{P}{8\pi}\left(2\ln\left(R_\beta\right) - 1\right) + N_r^P \tag{A.12}$$

- At $r = R_\beta, M_{r_\gamma} = M_{r_\beta}$ therefore:

$$\left(\frac{D_{\gamma_{11}} + D_{\gamma_{12}}}{-2}\right)c_6 + \left(\frac{D_{\gamma_{11}} - D_{\gamma_{12}}}{R_\beta^2}\right)c_7 + \left(\frac{B_{\gamma_{11}} + B_{\gamma_{12}}}{2}\right)c_9 + \left(\frac{B_{\gamma_{12}} - B_{\gamma_{11}}}{R_\beta^2}\right)c_{10} +$$
$$\left(\frac{D_{\beta_{11}} + D_{\beta_{12}}}{2}\right)c_{11} - \left(\frac{D_{\beta_{11}} - D_{\beta_{12}}}{R_\beta^2}\right)c_{12} - \left(\frac{B_{\beta_{11}} + B_{\beta_{12}}}{2}\right)c_{14} - \left(\frac{B_{\beta_{12}} - B_{\beta_{11}}}{R_\beta^2}\right)c_{15} =$$
$$\left[\left(\frac{B_{\beta_{11}}B_{\beta_{11}} - A_{\beta_{11}}D_{\beta_{11}}}{A_{\beta_{11}}D_{\beta_{11}} - B_{\beta_{11}}^2}\right) - \left(\frac{B_{\gamma_{11}}B_{\gamma_{11}} - A_{\gamma_{11}}D_{\gamma_{11}}}{A_{\gamma_{11}}D_{\gamma_{11}} - B_{\gamma_{11}}^2}\right)\right]\frac{P}{8\pi}\left(2\ln\left(R_\beta\right)+1\right) +$$
$$\left[\left(\frac{B_{\beta_{11}}B_{\beta_{12}} - A_{\beta_{11}}D_{\beta_{12}}}{A_{\beta_{11}}D_{\beta_{11}} - B_{\beta_{11}}^2}\right) - \left(\frac{B_{\gamma_{11}}B_{\gamma_{12}} - A_{\gamma_{11}}D_{\gamma_{12}}}{A_{\gamma_{11}}D_{\gamma_{11}} - B_{\gamma_{11}}^2}\right)\right]\frac{P}{8\pi}\left(2\ln\left(R_\beta\right)-1\right) + M_r^P \quad \text{(A.13)}$$

- At $r = R_\alpha, w_\beta = w_\alpha$ therefore:

$$c_{11}\frac{R_\alpha^2}{4} + c_{12}\ln\left(R_\alpha\right) + c_{13} - c_{16}\frac{R_\alpha^2}{4} - c_{18} =$$
$$\left[\left(\frac{A_{\alpha_{11}}}{A_{\alpha_{11}}D_{\alpha_{11}} - B_{\alpha_{11}}^2}\right) - \left(\frac{A_{\beta_{11}}}{A_{\beta_{11}}D_{\beta_{11}} - B_{\beta_{11}}^2}\right)\right]\frac{P}{8\pi}R_\alpha^2\left(\ln\left(R_\alpha\right)-1\right) \quad \text{(A.14)}$$

- At $r = R_\alpha, \frac{dw_\beta}{dr} = \frac{dw_\alpha}{dr}$ therefore:

$$c_{11}\frac{R_\alpha}{2} + c_{12}\frac{1}{R_\alpha} - c_{16}\frac{R_\alpha}{2} =$$
$$\left[\left(\frac{A_{\alpha_{11}}}{A_{\alpha_{11}}D_{\alpha_{11}} - B_{\alpha_{11}}^2}\right) - \left(\frac{A_{\beta_{11}}}{A_{\beta_{11}}D_{\beta_{11}} - B_{\beta_{11}}^2}\right)\right]\frac{P}{8\pi}R_\alpha\left(2\ln\left(R_\alpha\right)-1\right) \quad \text{(A.15)}$$

- At $r = R_\alpha, u_\beta = u_\alpha$ therefore:

$$c_{14}\frac{R_\alpha}{2} + c_{15}\frac{1}{R_\alpha} - c_{19}\frac{R_\alpha}{2} =$$
$$\left[\left(\frac{B_{\alpha_{11}}}{A_{\alpha_{11}}D_{\alpha_{11}} - B_{\alpha_{11}}^2}\right) - \left(\frac{B_{\beta_{11}}}{A_{\beta_{11}}D_{\beta_{11}} - B_{\beta_{11}}^2}\right)\right]\frac{P}{8\pi}R_\alpha\left(2\ln\left(R_\alpha\right)-1\right) \quad \text{(A.16)}$$

- At $r = R_\alpha, N_{r_\beta} = N_{r_\alpha}$ therefore:

$$\left(\frac{B_{\beta_{11}} + B_{\beta_{12}}}{-2}\right)c_{11} + \left(\frac{B_{\beta_{11}} - B_{\beta_{12}}}{R_\alpha^2}\right)c_{12} + \left(\frac{A_{\beta_{11}} + A_{\beta_{12}}}{2}\right)c_{14} + \left(\frac{A_{\beta_{12}} - A_{\beta_{11}}}{R_\alpha^2}\right)c_{15} +$$
$$\left(\frac{B_{\alpha_{11}} + B_{\alpha_{12}}}{2}\right)c_{16} - \left(\frac{A_{\alpha_{11}} + A_{\alpha_{12}}}{2}\right)c_{19} = \quad \text{(A.17)}$$
$$\left[\left(\frac{A_{\alpha_{12}}B_{\alpha_{11}} - A_{\alpha_{11}}B_{\alpha_{12}}}{A_{\alpha_{11}}D_{\alpha_{11}} - B_{\alpha_{11}}^2}\right) - \left(\frac{A_{\beta_{12}}B_{\beta_{11}} - A_{\beta_{11}}B_{\beta_{12}}}{A_{\beta_{11}}D_{\beta_{11}} - B_{\beta_{11}}^2}\right)\right]\frac{P}{8\pi}\left(2\ln\left(R_\alpha\right)-1\right) - N_r^P$$

- At $r = R_\alpha, M_{r_\beta} = M_{r_\alpha}$ therefore:

$$\left(\frac{D_{\beta_{11}} + D_{\beta_{12}}}{-2}\right)c_{11} + \left(\frac{D_{\beta_{11}} - D_{\beta_{12}}}{R_\alpha^2}\right)c_{12} + \left(\frac{B_{\beta_{11}} + B_{\beta_{12}}}{2}\right)c_{14} + \left(\frac{B_{\beta_{12}} - B_{\beta_{11}}}{R_\alpha^2}\right)c_{15} +$$
$$\left(\frac{D_{\alpha_{11}} + D_{\alpha_{12}}}{2}\right)c_{16} - \left(\frac{B_{\alpha_{11}} + B_{\alpha_{12}}}{2}\right)c_{19} =$$
$$\left[\left(\frac{B_{\alpha_{11}}B_{\alpha_{11}} - A_{\alpha_{11}}D_{\alpha_{11}}}{A_{\alpha_{11}}D_{\alpha_{11}} - B_{\alpha_{11}}^2}\right) - \left(\frac{B_{\beta_{11}}B_{\beta_{11}} - A_{\beta_{11}}D_{\beta_{11}}}{A_{\beta_{11}}D_{\beta_{11}} - B_{\beta_{11}}^2}\right)\right]\frac{P}{8\pi}\left(2\ln\left(R_\alpha\right)+1\right) +$$
$$\left[\left(\frac{B_{\alpha_{12}}B_{\alpha_{11}} - A_{\alpha_{11}}D_{\alpha_{12}}}{A_{\alpha_{11}}D_{\alpha_{11}} - B_{\alpha_{11}}^2}\right) - \left(\frac{B_{\beta_{11}}B_{\beta_{12}} - A_{\beta_{11}}D_{\beta_{12}}}{A_{\beta_{11}}D_{\beta_{11}} - B_{\beta_{11}}^2}\right)\right]\frac{P}{8\pi}\left(2\ln\left(R_\alpha\right)-1\right) - M_r^P \quad \text{(A.18)}$$

References

[1] Hansen C and Quake S R 2003 Microfluidics in structural biology: smaller faster ... better *Curr. Opin. Struct. Biol.* **13** pp 538-44

[2] Kumble K D 2003 Protein microarrays: a new tool for pharmaceutical development *Anal. Bio. Chem.* **377** 5 pp 812-19

[3] Willenbacher N and Oelschlaeger C 2007 Dynamics and structure of complex fluids from high frequency mechanical and optical rheometry *Curr. Op. Coll. Int. Sci.* **12** pp 43-9

[4] Ashkin A, Dziedzic J M, Bjorkholm J E and Chu S 1986 Observation of a single-beam gradient force optical trap for dielectric particles *Opt. Lett.* **11** pp 288–90

[5] Mukhopadhyay A and Granick S 2001 Micro- and nanorheology *Curr. Op. Coll. Int. Sci.* **6** pp 423-29

[6] Chu B 1992 *Laser Light Scattering: Basic Principles and Practice* 2nd Edition. Academic Press

[7] Weitz D A and Pine D J 1993 Diffusing-wave spectroscopy In: Brown W editor *Dynamic Light Scattering: the Method and some Applications* Oxford: Oxford University Press pp 652-720

[8] Crecea V et al. 2009 Magnetomotive nanoparticle transducers for optical rheology of viscoelastic materials *Optics Express* **17** 25 pp 23114-22

[9] Sujatha K S et al. 2008 Modelling Step-strain filament-stretching CaBER-type using ALE techniques *J. Non-Newtonian Fluid Mech.* **148** pp 109-21

[10] McKinley G H and Sridhar T 2002 Filament-stretching rheometry of complex fluids *Annu. Rev. Fluid Mech.* **34** pp 375–415

[11] Burnham N A and Colton R J 1989 Measuring the nanomechanical properties and surface forces of materials using an atomic force microscope *J. Vacuum Sci. Technol. A* **7** pp 2906-13

[12] Friedenberg M C and Mate C M 1996 Dynamic viscoelastic properties of liquid polymer films studied by atomic force microscopy *Langmuir* **12** pp 6138-42

[13] Kwok P Y, Weinberg M S and Breuer K S 2005 Fluid effects in vibrating micromachined structures *J. Microelectromechanical Sys.* **14** 4 pp 770-81

[14] Field J S, Swain M V and Phan-Thein N 1996 An experimental investigation of the use of random squeezing to determine the complex modulus of viscoelastic fluids *J. Non-Newtonian Fluid Mech.* **65** pp 177-94

[15] Crassous J J et al. 2005 Characterization of the viscoelastic behavior of complex fluids using the piezoelastic axial vibrator *J. Rheo.* **49** 4 pp 851-63

[16] Meeten G H 2002 Constant-force squeeze flow of soft solids *Rheol. Acta* **41** pp 557-66

[17] Cheneler D, Ward M C L, Adams M J et al. 2008 Measurement of dynamic properties of small volumes of fluid using MEMS *Sensors and Actuators B: Chemical* **130** 2 pp 701-6
[18] Madou M 1997 *Fundamentals of Microfabrication* CRC Press Florida US
[19] Deshpande M and Saggere L 2007 An analytical model and working equations for static deflections of a circular multi-layered diaphragm-type piezoelectric actuator *Sensors and Actuators A: Physical* **136** pp 673-89
[20] Ventsel E 2001 Thin *Plates and Shells: Theory Analysis and Applications* Marcel Dekker New York
[21] Ferry J D 1980 *Viscoelastic Properties of Polymers* 3rd Ed. Wiley New York
[22] Cheneler D, Bowen J, Ward M C L and Adams M J 2010 Micro squeeze flow rheometer for high frequency analysis of nano-litre volumes of viscoelastic fluid *Microelect. Eng.: The 36th International Conference on Micro- and Nano-Engineering (MNE)* in press
[23] Macosko C W 1994 *Rheology: Principles, Measurements, and Applications* Wiley-VCH Canada
[24] Dvornic P R, Jovanovich J D and Govedarica M N 1993 On the critical molecular chain length of polydimethylsiloxane *J. Appl. Polym. Sci.* **9** pp 1497-507